H_2 and D_2 in intense sub-picosecond laser pulses: Photoelectron spectroscopy at 1053 and 527 nm

H. Rottke, J. Ludwig, and W. Sandner
Max-Born Institut, Rudower Chaussee 6, P. O. Box 1107, D-12474 Berlin, Germany
(Received 3 January 1996)

We report multiphoton ionization experiments on H_2 and D_2 molecules at 1053- and 526.5-nm excitation wavelengths in the intensity range 5×10^{13}–5×10^{14} W/cm^2. The intensity dependence of the total ion yield, the dissociation fraction, and the photoelectron spectrum is investigated. At 1053 nm we find a strong isotope effect in the dissociation fraction, whereas at 526.5 nm no such effect is observed. Up to 1×10^{14} W/cm^2 the photoelectron spectrum at 526.5 nm is dominated by resonant ionization processes via Rydberg states of the molecules. They are shifted into resonance at intensities above $\sim10^{13}$ W/cm^2. The spectra show that the potential energy curves of the resonant states must have a shape very similar to the corresponding ionic ones. They are therefore mainly determined by the dipole coupling between the ion core orbitals $1s\sigma_g$ and $2p\sigma_u$. At 1053 nm two photoionization regimes are observed: the multiphoton regime with Keldysh parameter $\gamma>1$ showing resonance ionization structures, and the tunnel regime ($\gamma<1$) at high intensity. The isotope effect in the dissociation fraction at 1053 nm has no influence on the shape of the corresponding photoelectron spectra at this wavelength. [S1050-2947(96)02808-9]

PACS number(s): 33.80.Rv, 33.80.Wz, 42.50.Hz

I. INTRODUCTION

The behavior of molecules in a high-intensity electromagnetic field in the optical frequency range is a field of active research. The interest focuses on an intensity regime where perturbation theory fails to account for the interaction process. Since the radiation field primarily couples to the electrons of the molecule, strong-field phenomena already observed in atoms, such as multiphoton ionization (MPI), above-threshold ionization (ATI), or tunnel ionization in a low-frequency radiation field, are also found in molecules [1–7]. In contrast to atoms, these electronic excitation processes are modified by nuclear dynamics in most experiments, since the duration of the shortest light pulses used is similar to the nuclear dynamics time scale. The extra molecular degrees of freedom also give rise to completely new types of high-intensity phenomena such as dissociation through bond softening [2,4,8], above-threshold dissociation (ATD) [2,4,8,9], multiphoton dissociation (MPD) [4,8,10], light-induced bound vibrational states [11,12], and dissociation through Coulomb explosion after ejection of at least two electrons ([13], and references cited therein).

Investigations have mainly been performed on diatomic or small polyatomic molecules. Hydrogen and its singly charged ion are the smallest and therefore simplest molecules to study. Their unperturbed structure is well known, so they may serve as model systems amenable also to theoretical investigations. All experiments on H_2 and D_2 start with multiphoton excitation of the molecule in its electronic ground state $X^1\Sigma_g^+$. The processes observed seem to indicate a two-step mechanism. First, H_2^+ or D_2^+ is produced through MPI of the neutral molecule near the equilibrium internuclear distance of the $X^1\Sigma_g^+$ electronic ground state. Nuclear dynamics influenced by the strong optical radiation field, ultimately leading to dissociation into charged fragments, seems to be restricted to the molecular ion [2,4,12]. In the laser field the electric-dipole-allowed transition between the ionic ground state $1s\sigma_g$ and the nearby excited state $2p\sigma_u$ has a profound influence on nuclear motion (see [14], and references cited therein). In the hydrogen ion ejection of the remaining electron through multiphoton absorption may happen besides dissociation. This leaves two bare nuclei behind at a certain internuclear distance which will then fly apart due to their mutual Coulomb repulsion. Fast ions observed in an experiment by Zavriyev *et al.* are thought to originate from this ionization process [12].

Besides electronic excitation during the interaction process with a high-intensity laser pulse, an alignment of the internuclear axis along the polarization vector of the radiation is observed for molecules [2,15]. In terms of perturbation theory this alignment may be understood as resulting from a torque exerted on the molecule by the external electric field via its anisotropic electric polarizability [16].

In this paper we report the results of ion yield measurements and photoelectron spectroscopy after multiphoton ionization or dissociation of the hydrogen isotopes H_2 and D_2. The wavelengths used are 1053 nm and 526.5 nm with laser pulse peak intensities reaching up to 5×10^{14} W/cm^2 in pulses with 0.7-psec pulse width. Of special importance to the present work are experimental investigations by Verschuur, Noordam, and van Linden van den Heuvell [1], Zavriyev *et al.* [2], and Yang *et al.* [4]. They used pulsed Nd:YAG (YAG denotes yttrium aluminum garnet) (1064 and 532 nm) and Nd:YLF (YLF denotes lithium yttnium fluoride) (1054 and 527 nm) laser radiation at wavelengths nearby for their MPI studies on H_2 and D_2. The decisive difference in our investigations is that all other experiments were done with a minimum laser pulse width of $\sim$50 psec, much longer than in our case. Concerning photoelectron spectroscopy, this means that we are working in the so-called ''short'' pulse regime of MPI. The kinetic energy of the photoelectrons we detect is the drift energy they have when they appear in the laser focal spot at a certain intensity level, without subsequent ponderomotive acceleration, while

the electrons detected in Refs. [1,2,4] have gained energy through ponderomotive acceleration in the laser beam (''long'' pulse regime). This means that depending on pulse duration more or less the complete quiver energy has been transformed into directed drift motion by the time they are detected outside the focal spot [17]. Hence in Refs. [1,2,4] the photoelectron spectra mainly show the H_2^+ or D_2^+ internal energy distribution after MPI, while our spectra map transient resonances which may be induced by ac Stark shifting states either in H_2 or D_2 molecules or in H or D atoms created by dissociation [17]. Additionally, the shorter light pulses in our experiment allow us to reach much higher intensities before saturation of the ionization and dissociation processes of the molecules sets in. Thus we have access to processes at intensities where, in the case of long pulses, complete depletion of the initial species prevents observation.

II. EXPERIMENT

The primary light source for the experiment consists of a Kerr lens mode-locked Ti:sapphire laser pumped by a cw argon-ion laser. The Ti:sapphire laser is tuned to deliver pulses at 1053 nm. They are amplified in a Ti:sapphire regenerative amplifier using the chirped pulse amplification technique (CPA). Pumping of the amplifier is done with the second harmonic radiation of a Q-switched Nd:YAG laser. After recompression the output of this amplifier consists of pulses with a nearly Gaussian pulse shape at 1053-nm center wavelength with a repetition rate of 10 Hz, about 1.2-mJ pulse energy, and ~0.6-psec pulse width. Radiation at 526.5 nm is generated by frequency doubling the output of the regenerative amplifier in a lithium-iodate crystal. The energy of these pulses reaches ~0.5 mJ at a pulse width similar to the IR pulses.

An achromatic lens with 160-mm focal length focuses the light down to a spot size 20 μm in diameter at 1053 nm and 10 μm at 526.5 nm in the interaction region with the hydrogen molecules which is located within an ultrahigh-vacuum (UHV) chamber. In the focal plane a peak intensity of $\sim 5\times 10^{14}$ W/cm^2 is reached in a nearly Gaussian transverse spatial profile of the laser beam. The light intensity in the focal spot is controlled by a half-wave plate followed by a polarizer.

The base pressure reached in the UHV chamber after baking is 1×10^{-10} Torr. This reduces background gas ionization in the laser focal spot to a tolerable amount even at the highest intensities reached. Photoion mass spectra of the residual gas taken at the highest laser intensity mainly show H_2O^+, OH^+, H^+, and O^+ ions from multiphoton ionization or dissociation of water molecules desorbing from the walls of the vacuum chamber. During experiments hydrogen or deuterium gas is introduced into the vacuum chamber through a precision leak valve up to a maximum pressure of $\sim 1\times 10^{-5}$ Torr.

Mass selective detection of photoions from multiphoton ionization or dissociation within the laser focal spot is done with the time-of-flight technique. The drift tube used in the experiments has a length of 350 mm. It also serves as a field-free time-of-flight analyzer for the kinetic energy of the photoelectrons created in the interaction process. The time of flight of the charged particles is measured with a time-to-digital converter capable of accepting multiple stops per laser shot. The time resolution of this device is 1 nsec. The spectrometer has an energy resolution of ~20 mV for 0.5-eV electrons which decreases proportional to $E^{3/2}$ with increasing electron energy E. The acceptance solid angle of the microchannel plates used for photoelectron detection is 10^{-2} sterad. This limits the present angular resolution of the instrument to 6°. The whole spectrometer is housed within a double μ-metal shield to reduce the earth magnetic field along the drift path of the photoelectrons.

Calibration of the electron time-of-flight spectrometer is done through MPI of xenon using 532-nm laser radiation with nsec pulse duration and the amplified 526.5-nm, 0.6-psec pulses of the Ti:sapphire laser system. The kinetic energy spectra at 532 nm are well known. The absolute energy calibration was checked through three-photon resonant four-photon ionization of molecular hydrogen with rovibrational states of the B-electronic state as intermediate resonances. This MPI process gives rise to low-energy photoelectrons of precisely known kinetic energy.

The laser pulse width of ~0.6 psec in the experiment may give rise to residual ponderomotive acceleration of the photoelectrons. An estimate of the upper bound for the change in their kinetic energy by ponderomotive acceleration in the laser beam can easily be derived. The acceleration is largest in the focal plane in the direction perpendicular to the laser beam axis. If we assume a Gaussian beam and temporal pulse profile, maximum possible ponderomotive acceleration acting on the electron for the whole time from its creation to the end of the laser pulse, and creation of the photoelectron in the temporal pulse maximum we arrive at the relation

$$\Delta E/U_p = \pi/(8e)(U_p/E_b) + \sqrt{2\pi/e(E_0/E_b)} \qquad (1)$$

as the upper bound for the change $\Delta E/U_p$ of the electron kinetic energy relative to the pulse peak ponderomotive energy U_p. Here E_0 is the kinetic energy the photoelectron appears with in the laser focal spot, e the base of the natural logarithm, and E_b is defined by $E_b = m/2(d/\tau)^2$ with d the beam waist diameter [full width at half maximum (FWHM)], τ the pulse width (FWHM), and m the electron mass. E_b is a measure for the kinetic energy an electron must have to cross the laser beam within the laser pulse width. For 0.6-psec pulse duration E_b has the values 790 eV for the 527-nm laser beam and 3100 eV at 1053 nm. The different values have their origin in the different beam waist diameters. Relation (1) shows that $\Delta E/U_p$ grows proportional to the ponderomotive potential U_p and proportional to the square root of the initial kinetic energy E_0 of the photoelectron. Under our experimental conditions the second term in (1) dominates the change in photoelectron kinetic energy by ponderomotive acceleration.

III. RESULTS

A. The total ion yield

We measured the dependence of the total yield of photoions generated in the multiphoton excitation process of hydrogen and deuterium on the light intensity in the laser focal spot at the wavelengths 526.5 and 1053 nm. The intensity

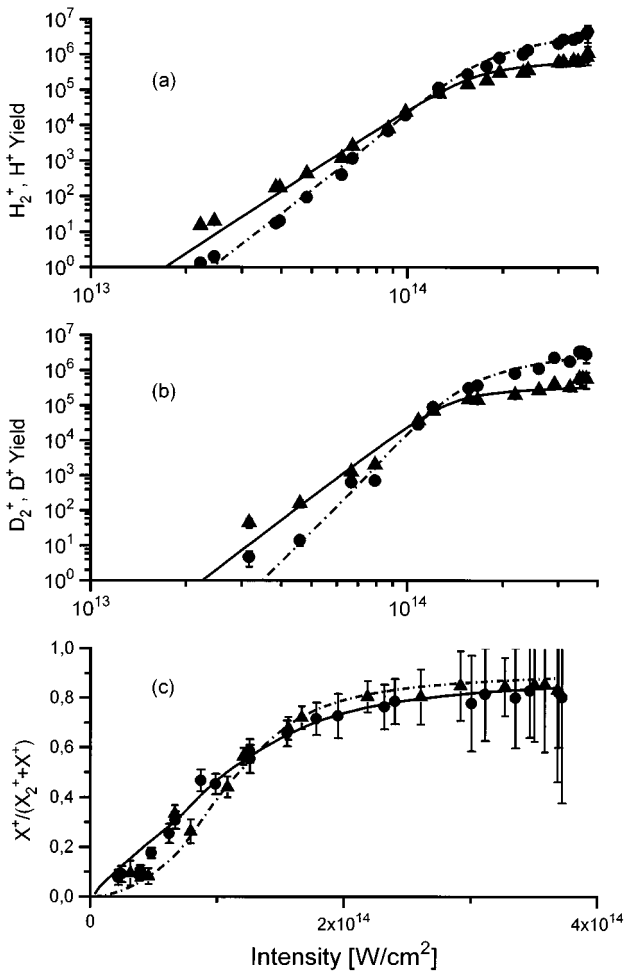

FIG. 1. The integral ion yield at 526.5-nm excitation wavelength with 0.77-psec laser pulses. (a) H_2^+ (triangles) and H^+ (circles) yield, (b) D_2^+ (triangles) and D^+ (circles) ion yield. The lines are the result of a model calculation. (c) shows the dissociation fraction for H_2 (circles) and D_2 (triangles) multiphoton excitation with the lines from the model calculation (dotted line, D_2 dissociation fraction).

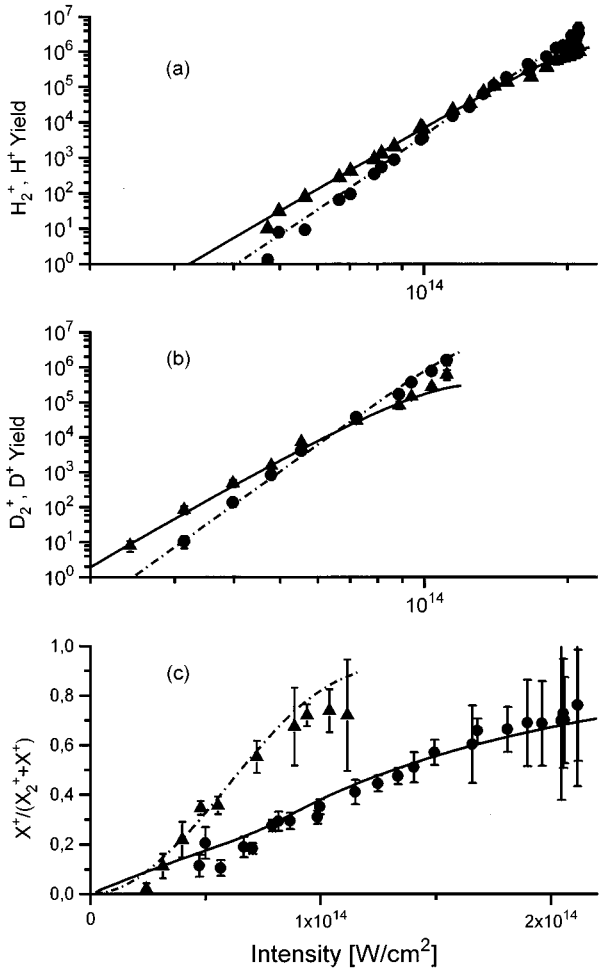

FIG. 2. The integral ion yield at 1053-nm excitation wavelength with 0.6-psec laser pulses. (a) H_2^+ (triangles) and H^+ (circles) yield, (b) D_2^+ (triangles) and D^+ (circles) ion yield. The lines are the result of a model calculation. (c) shows the dissociation fraction for H_2 (circles) and D_2 (triangles) multiphoton excitation with the lines from the model calculation (dotted line, D_2 dissociation fraction).

range covered is 2×10^{13}–4×10^{14} W/cm^2 at 526.5 nm and 3×10^{13}–2×10^{14} W/cm^2 at 1053 nm. H_2^+, D_2^+ and the charged dissociation products H^+, D^+ are detected mass selectively. Nearly equal collection efficiency for molecular and atomic ions is gained by choosing the polarization direction of the linearly polarized laser beam parallel to the mass spectrometer axis and extracting ions from the interaction region with a 250-V/cm electric field. This choice of polarization leads to a preferential direction of emission of the dissociation products along the spectrometer axis [2] and thus to the best collection efficiency. At the end of the drift tube the ions are further accelerated to 2-keV final energy. With this energy they hit the multichannel plate (MCP) detector. Since we are doing single ion counting we are sure that at this kinetic energy the detection efficiency for molecular and atomic ions is nearly the same [18].

The results at 526.5 nm are shown in Figs. 1(a) and 1(b) and at 1053 nm in Figs. 2(a) and 2(b) [(a) H_2 and (b) D_2 multiphoton excitation, respectively)]. The error bars in the figures indicate the statistical error in the number of detected ions. We were able to measure the yield over six orders of magnitude in the ion signal. In the visible (526.5 nm) the molecular and atomic yields clearly begin to saturate above $\sim1.5\times10^{14}$-W/cm^2 laser intensity whereas in the IR (1053 nm) saturation just sets in at the highest intensity available. In the visible the atomic ion yield overtakes the molecular ion yield near the saturation threshold, at the same intensity (1.2×10^{14} W/cm^2) for H_2 and D_2. The situation is completely different in the IR; here the atomic ion yield rises above the molecular one at $\sim7\times10^{13}$ W/cm^2 for D_2 and $\sim1.4\times10^{14}$ W/cm^2 for H_2, respectively.

Comparing the dissociation fraction for the two isotopes, the difference between the excitation processes at the two wavelengths becomes even more obvious. It is defined as the ratio $X^+/(X^+ + X_2^+)$ (with X=H or D) [2]. This ratio is shown in Fig. 1(c) for 526.5-nm and in Fig. 2(c) for 1053-nm excitation as a function of laser intensity. In the visible the dissociation fractions for H_2 (triangles) and D_2 (circles) are nearly equal over the whole intensity range investigated. If at all the ratio for D_2 is slightly higher than for H_2 for high intensity and slightly lower in the low-intensity regime. Both ratios approach a limiting value of $\sim$0.81 above about

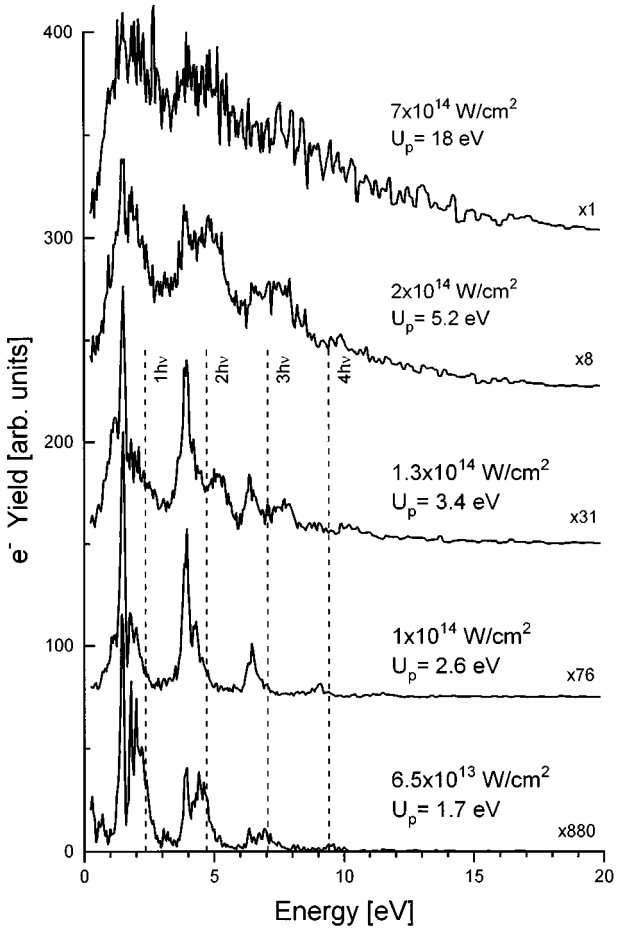

FIG. 3. Intensity dependence of the photoelectron kinetic energy spectrum for H_2 multiphoton excitation at 526.5 nm ($h\nu = 2.355$ eV) with 0.7-psec laser pulses. The laser pulse peak intensity and corresponding ponderomotive potential U_p are given on each spectrum. The number on the right hand side gives the signal scaling factor with respect to the highest-intensity spectrum. The dotted lines at multiples of the photon energy indicate the border between successive ATI orders.

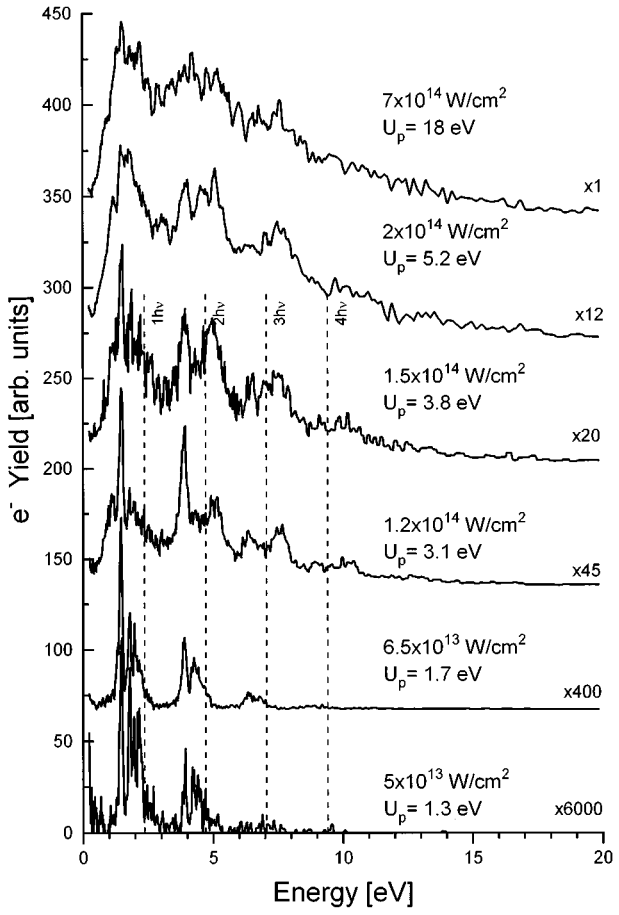

FIG. 4. Intensity dependence of the photoelectron kinetic energy spectrum for D_2 multiphoton excitation at 526.5 nm ($h\nu = 2.355$ eV) with 0.6-psec laser pulses. For other notation please refer to Fig. 3.

2.5×10^{14} W/cm^2. At 1053 nm the dissociation fraction for D_2 rises much faster than that for H_2 [Fig. 2(c)]. It reaches 0.75 as its highest value already at 1×10^{14} W/cm^2 which for H_2 is reached only at 2×10^{14} W/cm^2. At this wavelength an asymptotic value is not reached in the intensity range investigated. Both dissociation fractions are rising nearly linearly with intensity.

B. Photoelectron spectra

Photoelectron spectra were taken at 526.5- and 1053-nm excitation wavelengths for hydrogen and deuterium with the laser radiation linearly polarized along the axis of the time-of-flight energy analyzer. In Fig. 3 the H_2 spectra at 526.5 nm are shown for several values of the laser intensity in the range from 6.5×10^{13} up to 7×10^{14} W/cm^2, covering a regime from well below the saturation intensity for the excitation processes to far above. The laser pulse width for these experimental runs was kept fixed at 0.7 psec. At all intensities we took care to adjust the hydrogen density in the focal spot to a value where no influence of space charge on the electron kinetic energy was detectable. A similar set of spectra for D_2 at 526.5-nm excitation wavelength is shown in Fig. 4 covering a similar intensity range. They were taken at a slightly lower laser pulse width of 0.6 psec. At every spectrum we noted the laser pulse peak intensity, the corresponding maximum ponderomotive energy U_p for a free electron at this intensity, and a scaling factor to allow a direct quantitative comparison of the spectra. It is chosen as one ($\times1$) at the highest excitation intensity in each set of spectra.

The photoelectron spectra are taken in the short pulse regime but a residual ponderomotive acceleration of the photoelectrons remains due to the finite laser pulse width and small focal spot diameter. To get a feeling for the change in kinetic energy of the electrons, relation (1) can be employed to estimate the upper bound. The second term in (1) gives the main contribution to $\Delta E/U_p$. For the spectra in Fig. 3 (526.5-nm excitation) one derives, for example, $\Delta E/U_p = 9\%$ for 2-eV photoelectrons, 14% for 5-eV, and 20% for 10-eV photoelectrons. The ponderomotive acceleration will tend to broaden structures in the spectra with the upper bound for the broadening given by expression (1). For the example (Fig. 3) a structure at 2-eV kinetic energy and $U_p = 3.4$ eV (middle spectrum) may gain a width through ponderomotive acceleration which should be smaller than 300 meV, while at 5-eV kinetic energy and $U_p = 18$ eV (up-

permost spectrum) one expects 2.5 eV as upper bound for the broadening. Thus at the highest laser intensity used at 526.5 nm already an appreciable change in electron energy by ponderomotive acceleration may be expected. At this intensity one is leaving the short pulse regime for MPI already for quite slow photoelectrons.

At 526.5 nm the H_2 and D_2 photoelectron spectra look very similar in detail. This means that they are determined by the electronic structure of the molecules alone. The differing nuclear motion in the two isotopomeres which, for example, results in different vibronic and rotational structures seems to have only a negligible influence on the photoelectron spectra under our experimental conditions. Therefore we will restrict ourselves to analyzing the H_2 spectrum.

The kinetic energy distribution of the photoelectrons at the visible excitation wavelength changes strongly with increasing intensity. At low intensities, up to $\sim 1\times10^{14}$ W/cm^2, regularly spaced groups of photoelectrons appear. They show, at least at the two lowest intensities, a partly resolved resonance substructure with one resonance in each group dominating with increasing intensity. In the lowest-energy group the three unambiguously identifiable resonances appear at 1.47, 1.8, and 2.0 eV. Taking into account the decreasing resolution of our time-of-flight energy analyzer with increasing kinetic energy of the electrons the substructure of the two lowest-energy electron groups looks very similar up to an intensity of 1×10^{14} W/cm^2. To reveal the ''periodicity'' of the regularly spaced electron groups with the photon energy $h\nu=2.355$ eV we have added the vertical dashed lines to Figs. 3 and 4 at the positions $mh\nu$ with $m=1,\ldots,4$.

In the intermediate-intensity range (1×10^{14}–2×10^{14} W/cm^2) two new ''resonance'' structures appear at electron energies 5 and 7.5 eV. Their width increases with rising laser pulse peak intensity. The increase in width may at least partly be attributed to residual ponderomotive acceleration of the photoelectrons. The low-intensity structure in the spectra begins to vanish, only the strong resonance at 1.47 eV is perceptible up to about 2×10^{14} W/cm^2. Above this intensity a reproducible narrow linewidth structure is no longer present in the photoelectron spectra. Only three broad humps remain visible in the energy range from 0 to 10 eV. Above 10 eV a structureless tail develops with rising pulse peak intensity which reaches out to about 20 eV kinetic energy at the highest intensity available in our experiment.

The infrared (1053 nm) photoelectron spectra are shown in Fig. 5 for hydrogen and in Fig. 6 for deuterium. The intensity range covered here reaches from 2.5×10^{13} W/cm^2 up to 3.5×10^{14} W/cm^2. The notation used in these figures is the same as in Figs. 3 and 4. Above about 1×10^{14} W/cm^2 the photoelectrons are distributed over a broad featureless hump extending out to $\sim$80 eV for the highest intensity available. Comparing Figs. 3 and 4 with Figs. 5 and 6 one notes that at all comparable intensities the 1053-nm spectra extend over a much broader range of kinetic energies than the 526.5-nm ones do. At low intensity (up to $\sim 8\times10^{13}$ W/cm^2) the spectra show reproducible structures in the energy range below 10 eV. In these spectra the vertical lines at the positions $mh\nu$ ($h\nu=1.177$ eV, the photon energy, $m=1,\ldots,8$) separate regions where the photoelectrons have absorbed at least m photons in the ionization continuum. We added these lines to indicate that the structures are bound to intervals equal to the photon energy $h\nu$.

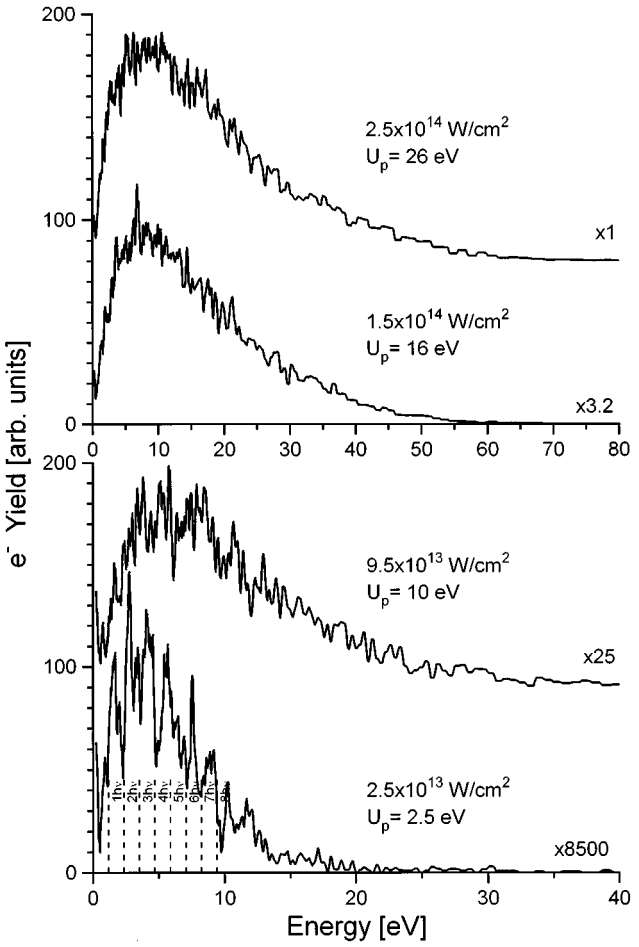

FIG. 5. Photoelectron kinetic energy spectra for H_2 multiphoton excitation at 1053 nm ($h\nu=1.177$ eV) with 0.6-psec laser pulses measured for different laser pulse peak intensities. For other notation please refer to Fig. 3.

At 1053 nm, modification of the kinetic energy of the photoelectrons by ponderomotive acceleration is less critical. Compared to 526.5 nm the energy they can gain is a factor of 2 smaller at a given electron kinetic energy E_0 and ponderomotive potential U_p. The reason for this behavior is the larger diameter of the focal spot which results in a higher value for E_b in relation (1).

IV. DISCUSSION

A. The total ion yield

Looking at the intensity dependence of the dissociation fraction for hydrogen and deuterium [Figs. 1(c) and 2(c)] the most striking difference between the 526.5- and 1053-nm data is the isotope sensitivity of this parameter at 1053 nm, whereas at 526.5 nm no such sensitivity is detected. This seems to indicate that it is only at the IR wavelength that nuclear dynamics strongly affects the generation mechanism of molecular and/or atomic ions. Different nuclear dynamics in H_2 and D_2 or H_2^+ and D_2^+, respectively, is exclusively caused by the different masses of the nuclei. It results in different nuclear velocities at a given total energy or, in the

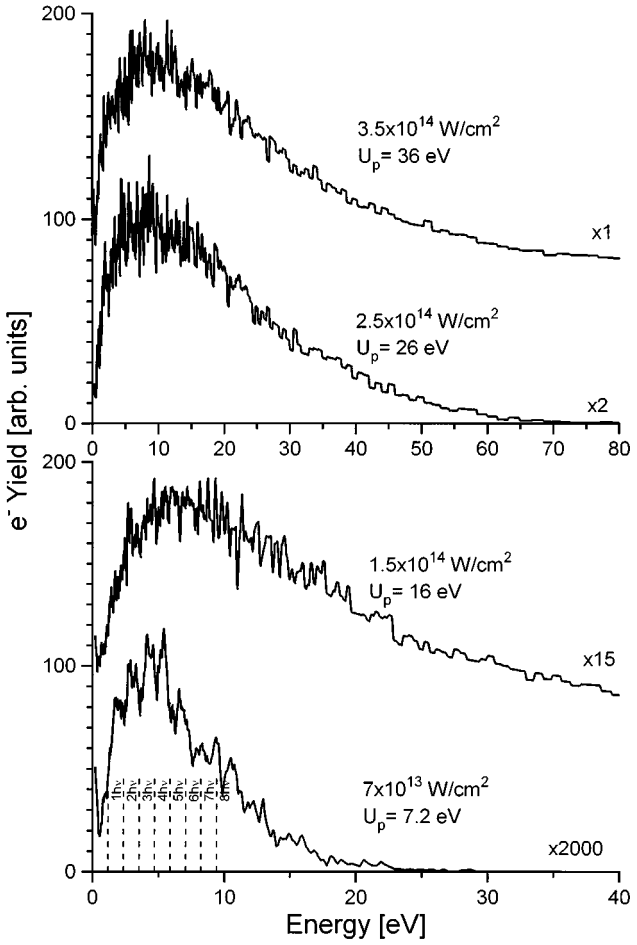

FIG. 6. Photoelectron kinetic energy spectra for D_2 multiphoton excitation at 1053 nm ($h\nu = 1.177$ eV) with 0.6-psec laser pulses measured for different laser pulse peak intensities. For other notation please refer to Fig. 3.

unperturbed molecule, leads to a closer vibrational and rotational energy level spacing in deuterium compared to hydrogen. The electronic properties of both molecules (i.e., potential energy curves) are identical.

Nuclear motion can have a strong influence on charged fragment generation if the generation mechanism is sensitive to the internuclear separation. This, for example, would be the case if excitation to the open fragmentation channel is localized at a certain internuclear distance, determined by the electronic properties of the molecule or molecular ion alone. D_2 or D_2^+, due to slower nuclear motion, would spend more time near the optimum internuclear distance than H_2 or H_2^+ and would therefore be dissociated with a higher probability. The initial vibronic wave function of D_2 in the electronic ground state is localized in a smaller range of internuclear distances than the corresponding $v=0$ H_2 wave function, namely, to ~84% of the H_2 range. We do not think that this different localization in the initial state gives rise to the strong isotope effect in the dissociation fraction and total ion yields at 1053 nm because we would expect a similar effect at 526.5-nm excitation wavelength.

Our data for the H_2 dissociation fraction can be compared with results of Zavriyev *et al.* at 1064-nm excitation wavelength with 70–100-psec laser pulses, that is, pulses about 100 times longer than those we used at practically the same wavelength [2]. Their data cover an intensity range from 3×10^{14} to 1×10^{15} W/cm^2. In this range the dissociation fraction rises from ~0.35 at the lower-intensity limit to ~0.81 where it levels off at high intensity. This behavior is completely different from what we measure [Fig. 2(c)]. In a lower-intensity regime the dissociation fraction rises nearly linearly from ~0.1 at 5×10^{13} W/cm^2 to ~0.7 near 2×10^{14} W/cm^2. Since the decisive difference between the experiments is the laser pulse width, this leads to the conclusion that the pathways leading to H_2^+ and/or H^+ are probably completely different in both experiments. They seem to depend sensitively on the laser pulse width. More detailed conclusions concerning these pathways, based only on these integral results, are not meaningful.

Contrary to our result at 526.5 nm, Yang and DiMauro find an isotope effect in the dissociation fraction at a slightly different wavelength (532 nm) [19], the fraction for D_2 is always higher than that for H_2. The main difference between their and our experiment is the lower-intensity range covered by Yang and DiMauro (1×10^{12}–3×10^{13} W/cm^2) and the laser pulse width (10 nsec). For our results this intensity range is completely unimportant. It does not contribute a detectable amount to the ion yield during excitation with sub-psec pulses even at the one to two orders of magnitude higher pulse peak intensities used in our experiment. The high-intensity level processes completely mask the low-intensity ones as will become clear in the discussion of the photoelectron kinetic energy spectra. This means Yang and DiMauro look at dissociation processes different from those we observe. At the higher-intensity level our results show a disappearance of the isotope effect in the dissociation fraction at 526.5 nm. This indicates that probably electronic properties alone determine the dissociation fraction at radiation intensities larger than 2×10^{13} W/cm^2.

All experiments done to date strongly indicate that the mechanisms responsible for generation of charged dissociation fragments in high-intensity multiphoton excitation of hydrogen or deuterium in the visible and near IR wavelength range are [2,4,12,19]

$$H_2 + mh\nu \rightarrow H_2^+ + e^-, \tag{2}$$

$$H_2^+ + nh\nu \rightarrow H(1s) + H^+, \tag{3}$$

$$H(1s) + lh\nu \rightarrow H^+ + e^-, \tag{4}$$

$$H_2^+ + kh\nu \rightarrow H^+ + H^+ + e^-. \tag{5}$$

This means dissociation starts after ionization of the neutral molecule. Dissociation of the neutral molecule would always result in at least one excited atomic fragment with immediate ionization of this fragment at the high-intensity levels used. Such a channel for charged fragment generation has not yet been found experimentally. After molecular ionization (2) dissociation yielding H^+ or D^+ may either proceed via process (3) with subsequent multiphoton ionization of the neutral ground-state atom $H(1s)$ [process (4)] or directly through process (5), that is, MPI of H_2^+ at a certain internuclear distance and subsequent Coulomb explosion of the bare nuclei. Process (3) seems to be active at an intermediate laser

TABLE I. Saturation intensities at 526.5 and 1053 nm in multiples of 10^{14} W/cm^2 for processes (2) and (3) of the rate model used to fit the experimental data for the total ion yield. The numbers n give the order of nonlinearity for the best fit.

	H_2		D_2	
	Process (2)	Process (3)	Process (2)	Process (3)
526.5 nm	1.2 ($n=7$)	0.8 ($n=1$)	1.2 ($n=8$)	0.8 ($n=2$)
1053 nm	1.6 ($n=9$)	1.2 ($n=1$)	0.9 ($n=9$)	0.4 ($n=2$)

intensity level ($\sim 1\times10^{12}$–$\sim 1\times10^{14}$ W/cm^2) [2,4,19] while process (5) may play a role at intensities in excess of $\sim 1\times10^{14}$ W/cm^2, as experiments at ~800-nm excitation wavelength indicate [12,14].

Based on processes (2)–(4) above we tried to model the intensity dependence of the ion yield and dissociation fraction using rate equations. The intensity-dependent rates for molecular ionization (2) and dissociation of H_2^+(3) which are unknown have been chosen as simple power laws of the form aI^n where a and n are adjustable parameters and I stands for the laser intensity. The parameter n was restricted to integer values so that aI^n takes the form of a perturbative rate. The rate for ground-state atomic hydrogen MPI [process (4)] at 526.5-nm excitation wavelength was taken from a Floquet calculation done by Dörr [20]. At 1053 nm we used a rate derived from the long-wavelength approximation for atomic hydrogen MPI [21]. These rates contain no adjustable parameters. Thus the rate equations contain altogether four adjustable parameters to fit the result of the calculation to the experimental data. In the model we ignored process (5) above. At 526.5 nm and intensities larger than 8×10^{13} W/cm^2 this process is approximately included because of saturation of atomic hydrogen ground-state MPI. This means processes (3) and (4) taken together become equivalent to (5) approximated with the rate of process (3). The spatial and temporal intensity distribution in the laser beam is taken into account using Gaussian temporal and spatial profiles which constitute a very good fit.

Using optimized parameters the results of the model calculation are shown in Figs. 1 and 2 as lines. As one can see, they fit the experimental data very well. If one defines saturation intensities via the relation $a(I_{\rm sat})^n\tau_p=1$ where τ_p is the laser pulse width and $I_{\rm sat}$ the pulse peak intensity necessary for saturation, the parameters a for processes (2), (3) can be expressed by saturation intensities $I_{\rm sat}$. At 526.5 nm the best fit yields equal saturation intensities for H_2 and D_2 as expected from the nearly equal experimental intensity dependence of the dissociation fractions. The values are shown in the first row of Table I in multiples of 10^{14} W/cm^2 together with the nonlinearities n of the different processes used for the best fit given in parentheses. These nonlinearities for H_2 and D_2 ionization and dissociation differ by 1. If perturbation theory is still applicable at least at intensities below 1×10^{14} W/cm^2 the parameter n may tentatively be interpreted as the number of photons absorbed to ionize the neutral molecule [process (2)] and dissociate the ion [process (3)]. Thus ionization would be a seven- or eight-photon process and dissociation a one- or two-photon process. This result from integral yield measurements compares quite favorably with conclusions drawn by Yang and DiMauro concerning the order of processes (2) and (3) derived from photoelectron spectroscopy and ion kinetic energy spectroscopy [4]. At intensities below 3×10^{13} W/cm^2 and an excitation wavelength equal to ours they conclude that H_2 ionization is an eight-photon process followed by dissociation of H_2^+ mainly via one-photon absorption. Better insight into the order of at least the H_2 ionization process will be gained from the photoelectron spectra.

At 1053-nm excitation wavelength (Fig. 2) the best fit parameters for the model calculation for H_2 and D_2 are different. They are shown in the second row of Table I. For H_2 one gets $I_{\rm sat}=1.6\times10^{14}$ W/cm^2 and $n=9$ for process (2) and $I_{\rm sat}=1.2\times10^{14}$ W/cm^2 and $n=1$ for process (3), while for D_2 $I_{\rm sat}=9\times10^{13}$ W/cm^2 and $n=9$ [process (2)] and $I_{\rm sat}=4\times10^{13}$ W/cm^2, $n=2$ [process (3)]. At this wavelength the saturation regime is only touched at the highest intensities available. Therefore the values derived for $I_{\rm sat}$ are less reliable than those at 526.5 nm.

It is interesting to see that the saturation intensities necessary to assume for the best fits to the experimental data are always higher for H_2 or D_2 ionization than for H_2^+ or D_2^+ dissociation, at 526.5 nm as well as for 1053 nm. Only this choice of $I_{\rm sat}$ ensures that above a certain intensity the H^+ or D^+ yield overtakes the H_2^+ or D_2^+ yield. This has a strong effect on the molecular ion states which serve as initial states for dissociation. They are already strongly perturbed by the laser field at the time when they are populated through MPI of the neutral molecule during the laser pulse. It may even be that under our experimental conditions, at both wavelengths investigated, the molecule is ionized directly into the dissociation continuum of light-perturbed electronic states.

B. 526.5-nm photoelectron spectra

The photoelectron spectra give a far more detailed insight into the molecular processes in the high-intensity laser field than the integral yield measurements can. Especially at 526.5-nm excitation wavelength the resonance structure observed for intensities below $\sim 1.5\times10^{14}$ W/cm^2 is very helpful (Figs. 3 and 4). Its appearance signals that the processes may be analyzed within the framework of multiphoton absorption; the low-frequency approximation which describes ionization by a tunnel mechanism is not applicable. We will first discuss the 526.5-nm spectra in the intensity regime below 1.0×10^{14} W/cm^2 in detail using the H_2 data (Fig. 3). Most of the results can then be transferred to D_2 as long as vibrational and rotational structures of the molecules are not involved.

As already noted above, we are in the short-pulse regime of MPI. Therefore, most of the structure in Figs. 3 and 4 is

generated through transient resonances induced by ac Stark shifting states. Resonances appear when the intensity-dependent energy separation $E_f(I)-E_i(I)$ between the initial and an excited state equals an integer multiple of the photon energy [17]. At such an intensity the ionization rate is enhanced. The resonance enhancement appears in the photoelectron spectrum at a specific electron kinetic energy $E_{\rm kin}(I)$ determined by the relation

$$E_{\rm kin}(I_{\rm res})=E_f(I_{\rm res})-E^+(I_{\rm res})+mh\nu-U_p(I_{\rm res}), \qquad (6)$$

where $E^+(I)$ is the energy of the final ionic state and $U_p(I)$ the quiver energy (ponderomotive energy) of the photoelectron released at the resonance intensity $I_{\rm res}$. The number of photons absorbed to ionize the system from the resonant excited state f is denoted by m. For m larger than the minimum number of photons necessary for ionization the photoelectron has absorbed photons in the ionization continuum (above threshold ionization). In Figs. 3 and 4 ATI electron groups are separated by the vertical dashed lines below 10 eV kinetic energy. Electrons in an energy interval $[kh\nu,(k+1)h\nu]$ $(k=0,1,\ldots)$ have absorbed k photons in the ionization continuum.

Before identifying the resonant states it is first necessary to specify the species responsible for the resonance structure. Possible candidates are H_2 and H atoms in the $1s$ ground state which may be created via either process (3) above or neutral dissociation. The process mentioned last cannot from the beginning be excluded despite the fact that up to now it has not been found in experiments at the excitation wavelength used [2,4,19]. Neutral dissociation will always leave the second atom in an excited state. If this atomic state has a principal quantum number larger than 2, absorption of one photon will suffice to ionize the atom, while for $n=2$ two photons are necessary. Ground-state atoms have to absorb at least six photons for ionization.

To check whether the atomic ground state $1s$ may be responsible for the structure in the photoelectron spectrum we compare in Fig. 7 the experimental spectrum in the energy range $[0,h\nu]$ (lowest ATI group) with a calculated H($1s$) MPI spectrum at an intensity 1×10^{14} W/cm^2 [20]. The calculation is based on the total ionization rate of the atomic ground state. It is therefore only good for locating resonances and revealing their widths; relative intensities of the resonances may be in error. The calculation definitely shows that the observed resonance at 1.47 eV ($E/h\nu=0.62$) is not an atomic one with the atomic ground state $1s$ as initial state. Therefore we conclude that H($1s$)/D($1s$) MPI is not responsible for the resonance structure observed for H_2 as well as for D_2 below 1×10^{14} W/cm^2.

The calculation of the spectrum assumes that H($1s$) atoms are present in the focal spot before the laser pulse arrives. This is certainly not the case in the experiment. H($1s$) there is formed at already elevated intensities by dissociation of H_2 or H_2^+. Therefore ionization of H($1s$) may not at all give rise to any resonance structure in the photoelectron spectrum. This would be the case if H($1s$) is efficiently created only at intensities higher than the highest resonance intensity ($\sim7\times10^{13}$ W/cm^2) and the saturation intensity $\sim8\times10^{13}$ W/cm^2 for H($1s$) ionization.

Neutral dissociation with H($n>2$) as one product channel subsequently ionized by one-photon absorption cannot be excluded by an argument based on the photoelectron spectrum (see, for example, Ref. [5]). For these states one would expect photoelectrons appearing approximately just at the positions where we observe the resonances. Here it is necessary to argue with the dissociation fraction we measured. At all laser intensities used, excited atomic states would immediately ionize because only one ($n>2$) or two photons ($n=2$) need to be absorbed. Therefore they all would contribute to the H^+ yield in the whole intensity range covered. The photoelectron spectra show that the lower the laser peak intensity is, the more prominent the resonance structure becomes. At the lowest intensity resonance structures even constitute the whole spectrum. On the other hand, the dissociation fraction [Fig. 1(c)] decreases with decreasing laser peak intensity, reaching ~0.1 at the lowest intensity used to record photoelectron spectra. This means even if all atomic ions detected originated from atomic ionization after neutral dissociation only $\sim10\%$ of the electrons in the photoelectron spectrum recorded at the lowest laser intensity can arise from atomic ionization. The main contribution to the resonance structure at low intensity is thus definitely molecular MPI, for H_2 as well as for D_2. The data thus strongly suggest that the process responsible for the resonance structure visible in the whole intensity range up to $\sim1\times10^{14}$ W/cm^2 is molecular MPI.

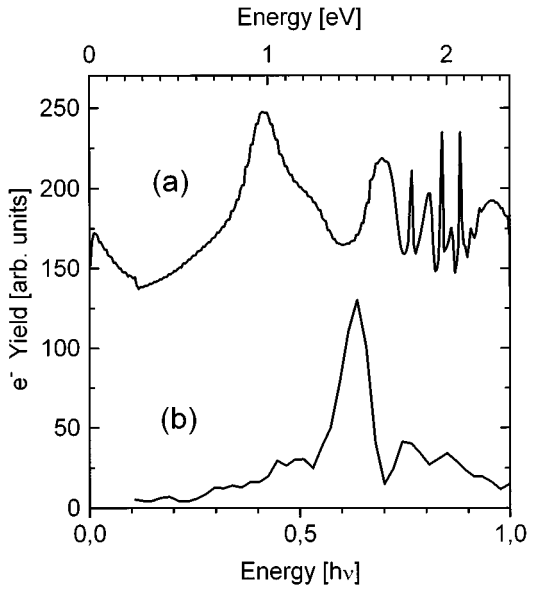

FIG. 7. Comparison between a calculated photoelectron spectrum of atomic hydrogen [20] (a) and a measured spectrum from H_2 multiphoton excitation (b) in the energy regime of the lowest ATI order. The kinetic energy is measured as a multiple of the photon energy. The calculation and experiment were done at 526.5 nm, 1×10^{14} W/cm^2 pulse peak intensity, 0.6-psec (calculation) and 0.7-psec (experiment) laser pulse width.

Analysis of the resonance positions in the energy interval $[0,h\nu]$ shows that they may be interpreted as members of a Rydberg series with principal quantum numbers $n=4,5,6$ (Fig. 8). Resonant excitation to these molecular Rydberg states requires the absorption of seven laser photons. Absorption of one further photon from the resonant state then suffices for ionization. This means the resonance structure in the energy intervals $[(m-1)h\nu,mh\nu]$ $(m=1,2,\ldots)$ we observe

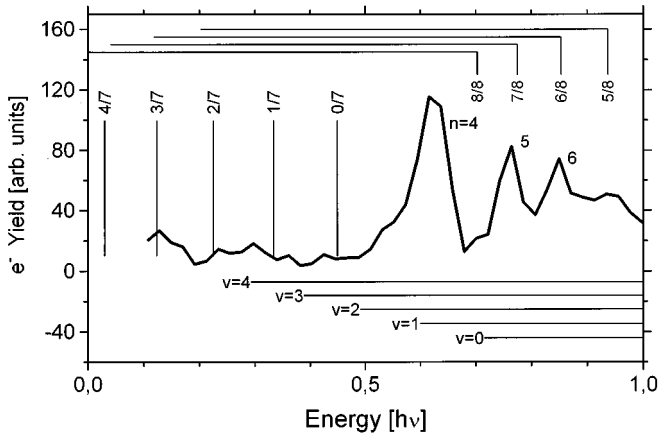

FIG. 8. Photoelectron spectrum for H_2 multiphoton excitation at 526.5 nm, 6.5×10^{13} W/cm^2 laser pulse peak intensity, and 0.7-psec pulse width. The intensity range of the lowest ATI order $[0,h\nu]$ is shown with the energy measured as a multiple of $h\nu$. $n=4,5,6$ numbers the principal quantum numbers of the identified Rydberg state resonances. For further details see the text.

in the intensity range up to 1×10^{14} W/cm^2 originates in seven-photon resonant $(7+m)$-photon ionization of molecular hydrogen and, similarly, deuterium.

The approximate calculation made to identify the resonant states uses for their intensity-dependent energy $E_f(I)=E^+(I)+U_p(I)-\mathcal{R}/n^2$ in relation (6) above (n principal quantum number of the excited resonant state, $\mathcal{R}=13.60$ eV Rydberg constant). This means the binding energy is approximated by the atomic hydrogen value $-\mathcal{R}/n^2$. With this simplification we expect resonances at 1.505 ($n=4$), 1.811 ($n=5$), and 1.977 eV ($n=6$). These values compare favorably with the measured ones at 1.47, 1.80, and 2.00 eV. Small deviations, even changing with the resonant state, may have their origin in the approximation used for $E_f(I)$. They should become increasingly important for stronger bound resonant states where the electron cannot yet respond to the light field in nearly the same way as a free one [assumed in the approximation for $E_f(I)$ above]. In addition, with decreasing principal quantum number n a growing deviation from the simple atomic hydrogen binding energy $-\mathcal{R}/n^2$ is to be expected, which should be enhanced by a low angular momentum of the electron in the resonant state. This point may justify us to speculate that the electron in the excited resonant state has a high angular momentum as it is observed for resonant states in atomic hydrogen MPI. Here f-angular momentum states play a prominent role [22].

The fact that the resonance spacing in the photoelectron spectrum follows that of a Rydberg series implies that the final state reached in the molecular ion after one-photon ionization is the same as the ion core state in the resonant state. For the vibrational degree of freedom this means that the ionic vibrational level must be identical to the resonant state vibrational level ($\Delta v=0$ ionizing transitions) otherwise the photoelectron spectrum would not have the simple structure observed. This definitely excludes non-Rydberg states of the molecule from being the resonant states. Only the unperturbed potential energy curves of Rydberg electronic states closely match the ionic $X^2\Sigma_g^+$ ground-state curve [23] and therefore guarantee $\Delta v=0$ transitions to dominate photoionization. In this case, irrespective of the vibrational quantum number v in the resonant electronic state the kinetic energy of the ejected electron is always the same, determined only by the principal quantum number n of the resonant state.

Zavriyev *et al.* investigated multiphoton excitation of H_2 with ~70-psec laser pulses at a nearby wavelength (532 nm) in the same intensity range as we did [2]. Similar to Verschuur, Noordam, and van Linden van den Heuvell [1] they suspect from their photoelectron spectra lower excited states of the molecule to become resonant during the laser pulse. These experiments were done in the ''long'' pulse regime. Therefore the authors had to judge from the internal energy distribution in the H_2^+ ion they measure with the photoelectron spectrum what the resonant states may be. Based on Franck-Condon overlap arguments, Zavriyev *et al.* favor vibrational levels of the $B^1\Sigma_u^-$ electronic state to become resonant after absorption of five photons with at least two further photons necessary for ionization. Our observations do not support this choice of resonant states. But this does not mean the conclusion of Zavriyev *et al.* is in error. The much faster rise time of our laser pulses may prefer the observed seven-photon resonances at a higher-intensity level within the pulses. Also Helm, Dyer, and Bissantz showed for UV multiphoton excitation of H_2 a quite strong wavelength dependence of the photoelectron spectra [5]. At two excitation wavelengths separated by only 7.5 nm the spectra show a quite strong structural change. Therefore even the small wavelength difference between 532 and 526.5 nm may change the resonant states relevant for the MPI process.

So far it has been shown that molecular Rydberg states are responsible for the resonance structure in the spectra and their principal quantum numbers were identified. We have not yet analyzed what the vibrational quantum numbers of the Rydberg states are. Depending on laser pulse peak intensity the vibrational states contributing to a resonance may change. For a closer examination of the resonance structure we have plotted the part of the H_2 photoelectron spectrum measured at 6.5×10^{13} W/cm^2 laser pulse peak intensity within the first ATI group (energy range $[0,h\nu]$) on an expanded scale in Fig. 8. The kinetic energy is given in multiples of the photon energy $h\nu$. The vertical lines labeled v/m indicate the kinetic energy a photoelectron would have if it were ionized by absorption of $m=7$ or 8 laser photons at zero intensity with the H_2^+ ion left in an unperturbed (zero intensity) vibrational state $v=0,1,2,\ldots$, respectively. With ionization proceeding at increasing laser intensity the kinetic energy of the released photoelectrons decreases until it reaches zero at a specific intensity which depends on the vibrational state of the ion. Thus seven-photon ionization contributes to the spectrum only in an energy range to the left of the vertical lines labeled $v/7$ when the ion is created in the vibrational state v. The only ionic vibrational channels open for seven-photon ionization are $v=0,\ldots,4$ for H_2. As can be seen in Fig. 8, the electron yield from seven-photon ionization is very small (energy range below 0/7). Contributions to the photoelectron spectrum from the lowest-order ionization process possible can thus completely be neglected at all intensities where we took spectra.

All ionic vibrational states with vibrational quantum number $v>4$ can in lowest order only be reached by absorption of eight photons. The labels $v/8$ with $v>4$ in Fig. 8 mark the

energy photoelectrons would have after eight-photon ionization at zero intensity for an ion core left in a vibrational state $v=5,6,\ldots$. With increasing intensity eight-photon ionization into these vibrational channels releases photoelectrons with decreasing kinetic energy. For 6.5×10^{13} W/cm^2 laser pulse peak intensity in Fig. 8 the horizontal lines attached to the left of the $v/8$ labels indicate the energy range where photoelectrons may be emitted with the ion core remaining in a $v>4$ state. In the energy region below $0.5h\nu$, corresponding to the highest intensity in the laser pulse, only a small electron yield is observed. This fact suggests concluding that eight-photon ionization into ionic vibrational states with $v>4$ only negligibly contributes to the photoelectron spectrum in the whole interval $[0,h\nu]$. Since up to $\sim1\times10^{14}$ W/cm^2 the resonance structure dominates the spectrum in $[0,h\nu]$ it may be justified to conclude that eight-photon ionization into $v>4$ and seven-photon ionization only play a minor role in this intensity regime.

When the seven-photon $v=4,\ldots,0$ ionization channels close at successively higher intensities the lowest-order ionization process becomes eight photon. At the channel closure intensity the kinetic energy of the photoelectrons released is $h\nu$ after absorption of eight photons. At higher intensities the electron energy decreases below $h\nu$. In Fig. 8 the horizontal lines labeled $v=0,\ldots,4$ below the spectrum mark the energy range where electrons can be created by eight-photon ionization with the ion left in the corresponding vibrational state noted. These lines terminate at the kinetic energy corresponding to the laser pulse peak intensity 6.5×10^{13} W/cm^2. Within this energy range ($[E_{\rm kin}(I_{\rm max}),h\nu]$) seven-photon absorption resonantly enhances the eight-photon ionization process. At the specific laser pulse peak intensity chosen $n=5,6$ Rydberg states with vibrational quantum numbers $v=0,\ldots,4$ may thus contribute to the resonances labeled $n=5,6$ whereas only $n=4$ Rydberg states with $v=1,\ldots,4$ may contribute to the $n=4$ resonance. At the higher laser peak intensities (Fig. 3) this situation changes of course; also the $n=4$, $v=0$ Rydberg state may then contribute to the resonance labeled $n=4$ in Fig. 8.

A Franck-Condon argument can be used to confirm that really all energetically accessible vibrational levels of a Rydberg electronic state will contribute to a resonance. Compared to the minima of the Rydberg state potentials, the minimum of the H_2 $X^1\Sigma_g^+$ ground-state potential energy curve is shifted to a smaller internuclear distance and the $X^1\Sigma_g^+$ potential well is much narrower [23]. Thus resonant transitions starting at the H_2 ground state $X^1\Sigma_g^+(v=0)$ to the Rydberg states have a high Franck-Condon factor for a broad distribution of vibrational states. Based on Franck-Condon factors for the Rydberg transition $C^1\Pi_u$-$X^1\Sigma_g^+(v=0)$ [24] one can approximately specify the general shape of their dependence on the Rydberg state vibrational quantum number v. After a first slight increase for $v=0,\ldots,2$ they reach a maximum at $v=2$. Then a very slow decrease sets in. Only at $v\sim10$, the Franck-Condon factors have diminished by about one order of magnitude. This strongly suggests that, if energetically allowed, all vibrational states $v=0,\ldots,4$ contribute to each resonance observed in the photoelectron spectra.

In the analysis up to this point we have neglected the dependence of the molecular potential energy curves and therefore also of the vibrational energy levels on the intensity of the radiation field [8–11,14]. The Rydberg states are shifted into resonance at intensities above $\sim1\times10^{13}$ W/cm^2. In this intensity range the adiabatic potential energy curves of the ion are heavily deformed by the interaction with the light field and so will be the potentials of the resonant Rydberg states. In the ion the relevant electronic states for the processes investigated here are the ground state $1s\sigma_g$ and the first excited repulsive state $2p\sigma_u$ [2,4,8–12,14]. They are strongly dipole coupled by the laser radiation. This implies that not only the molecular electronic states $(1s\sigma_g)(nl)$ but also the doubly excited configurations $(2p\sigma_u)(nl)$ have to be taken into account in the analysis of the resonant Rydberg states. They should be coupled by the radiation field in a way similar to the ionic states. The photoelectron spectra at 526.5 nm strongly suggest that at least the observed resonant electronic states have potential energy curves very similar to the corresponding ionic ones ($\Delta v=0$ transitions dominate) at the laser intensity where they are shifted into resonance. The coupling between the $(1s\sigma_g)(nl)$ and $(2p\sigma_u)(nl)$ states with fixed principal quantum number n induced by the radiation field is thus expected to be stronger than the coupling between at least the $n=4,5,6$ $(1s\sigma_g)(nl)$ configurations to other singly excited molecular hydrogen configurations.

To illustrate the strength of the dipole interaction between the ionic electronic states $1s\sigma_g$ and $2p\sigma_u$ we plotted in Fig. 9(a) the unperturbed adiabatic potential curves and in Fig. 9(b) the potentials in a radiation field (wavelength 526.5 nm) at an intensity 5×10^{13} W/cm^2. Here it is assumed that the polarization points along the internuclear axis. Adiabatic potentials in the radiation field are calculated using the Floquet method with seven Floquet blocks included in the length gauge [14]. The unperturbed potentials are taken from Sharp [23], and dipole coupling strengths between $1s\sigma_g$ and $2p\sigma_u$ from Ramaker and Peek [25]. In the figure we included the positions of unperturbed H_2^+ $X^2\Sigma_g^+$ vibrational levels with $v=0,\ldots,8$ (horizontal lines). As discussed above, the potential energy curves at least for the resonant Rydberg states identified in the electron spectra are expected to have a shape very similar to these ionic potentials.

Ignoring a three-photon avoided crossing between $1s\sigma_g$ and $2p\sigma_u$-$3h\nu$ near 2.75 a.u. the perturbed state labeled g in Fig. 9(b) is the $1s\sigma_g$ state for small internuclear distances (sufficiently far below the wide one-photon avoided crossing gap between $1s\sigma_g$ and $2p\sigma_u$-$h\nu$ near 4.2 a.u.) and the $2p\sigma_u$-$h\nu$ state at a sufficiently large internuclear distance. Following the corresponding potential energy curve adiabatically from small to large R leads to one-photon dissociation for energies above the barrier near 3.8 a.u. (bond softening [2]). Even dissociation by tunneling through the barrier may be possible for vibrational states below the top and above an energy D_0-$h\nu$ (D_0 unperturbed dissociation energy). As Fig. 9(b) shows, the adiabatic state g can probably support only three bound states with the highest one already amenable to tunnel dissociation at the intensity chosen. Above the top of the potential barrier a dissociation continuum persists for state g at this specific intensity. At lower light intensities the potential barrier in the g state rises so that more vibrational states become bound. The situation for the resonant Rydberg state potentials should look very similar to the ionic one in Fig. 9(b).

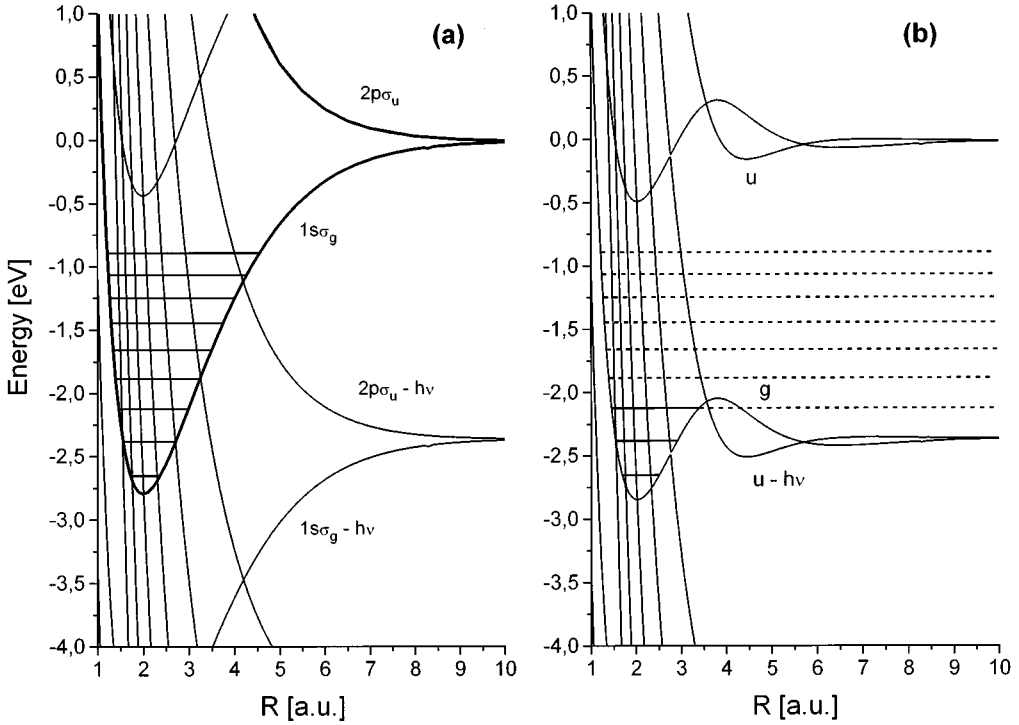

FIG. 9. Potential energy diagram for the two lowest-energy electronic states of the hydrogen ion. (a) Unperturbed adiabatic dressed potential energy curves ($h\nu = 2.355$ eV), (b) the adiabatic dressed curves at 5×10^{13} W/cm^2 radiation field intensity (light polarization assumed parallel to the internuclear axis). The horizontal lines show the position of the unperturbed ionic vibrational states for $v = 0,\ldots,8$.

Figure 9 shows that excitation from the molecular ground state $X^1\Sigma_g{}^+(v=0)$ whose vibrational wave function is located below $R\sim2$ a.u. to the Rydberg states has a large Franck-Condon factor only for states corresponding to the g ionic state with a small R potential nearly equal to the unperturbed $1s\sigma_g$ ionic potential. They will therefore be the resonant electronic states independent of the intensity where the excitation takes place, i.e., where a state shifts into seven-photon resonance. Bound vibrational states [for example, $v=0,1,2$ in Fig. 9(b)] or the dissociation continuum of a perturbed excited electronic Rydberg state may equally well enhance the ionization process. Even the dissociation continuum will lead to well-defined electron kinetic energies after one-photon ionization, since nuclear motion is not changed in the ionizing transition (nearly equal ionic and Rydberg potentials at the resonance intensity).

To conclude the discussion of the resonance structures in the photoelectron spectra at 526.5 nm it has been shown that even for resonant electronic states heavily perturbed by the radiation field the simple resonance structure observed in the experiment is to be expected. The only condition which must be met is that the potentials of the resonant and the ionic state are affected in nearly the same way by the radiation field. The same discussion applies to D_2 MPI and the resonances found there. The only difference is that the larger nuclear mass necessitates the inclusion of a broader range of vibrational states.

Starting at 1×10^{14} W/cm^2 the photoelectron spectra at 526.5 nm develop new features which bury the resonance structure with increasing intensity (see Figs. 3 and 4). In this regime the dissociation fraction is higher than 0.5, reaching nearly the saturation value 0.8 at $\sim2\times10^{14}$ W/cm^2 [see Fig. 1(c)]. Below the resonance structure in the lowest-order ATI photoelectron group (energy interval $[0,h\nu]$) a broad feature seems to develop, peaking at a kinetic energy slightly below the position of the $n=4$ resonance (see, for example, in Fig. 3 the 1.3×10^{14} W/cm^2 spectrum). A second main modification in the spectrum within the range 1×10^{14}–2×10^{14} W/cm^2 are two local electron yield enhancements slightly above $E_{\rm kin}=2h\nu$, $3h\nu$. A similar enhancement does not appear near $E_{\rm kin}=h\nu$. These features broaden slightly and increase in height with increasing laser intensity. They have a similar position shape and dependence on laser intensity for H_2 and D_2 MPI (Figs. 3 and 4). Since no isotope effect is found, these features seem to have a purely electronic origin. At the highest laser intensity the H_2 and D_2 electron spectra are mainly structureless; only two broad electron yield maxima are observed in the low-energy part.

There are a few points that make an interpretation of the spectra in the high-intensity range very difficult. The high dissociation fraction measured indicates that not only H_2 MPI contributes to the spectrum but possibly also MPI of possible H($1s$) dissociation products and MPI of $H_2{}^+$. All H($1s$) and, similarly, D($1s$) produced at intensities above $\sim8\times10^{13}$ W/cm^2 in the laser pulse (saturation intensity of ground-state hydrogen MPI for our pulse width) will certainly be ionized at the end of the pulse. The photoelectron spectrum alone does not allow us to distinguish between these ionization processes.

There are some hints in the spectra that H($1s$)/D($1s$) MPI may contribute. These are the yield enhancements slightly above $E_{\rm kin}=2h\nu$, $3h\nu$ in Figs. 3 and 4. Appreciable

H^+ or D^+ ion yield is found at laser pulse peak intensities above $\sim 1\times10^{14}$ W/cm^2 where the dissociation fraction has increased to about 0.4. This means that if dissociation into the channel $H(1s)+H^+$ occurs, $H(1s)$ will in an appreciable amount be produced at intensities above $\sim 1\times10^{14}$ W/cm^2. In this range the $H(1s)$ ionization rate is higher than $\sim 7\times10^{12}$ sec^{-1} [20]. At this rate, ionization of the atom will be complete in less than $\sim$150 fsec. When compared to our laser pulse width of 0.6–0.7 psec this implies that the intensity does not change very much over the time it takes the H atom to ionize if it is created through dissociation above $\sim 1\times10^{14}$ W/cm^2. Certainly only a few $H(1s)$ atoms will survive until the laser pulse reaches intensities well below 1×10^{14} W/cm^2 on the trailing edge where the main contribution to resonant ionization should have its origin. This means that $H(1s)$ ionization will mainly be nonresonant. If one therefore assumes that $H(1s)$ or $D(1s)$ gets completely ionized near an intensity of $\sim 1\times10^{14}$ W/cm^2 just after production it is possible to approximately determine the kinetic energy where photoelectrons from this process should appear. Taking into account a ponderomotive shift of the ionization threshold relative to the $1s$ ground state, a kinetic energy $mh\nu+0.3$ eV ($m=0,1,\ldots$) is calculated for photoelectrons which have absorbed m photons in the ionization continuum. For $m=2,3$ this is just the energy where we observe the local electron yield enhancements in the electron spectra (Figs. 3 and 4). We do not see an enhancement for $m=0,1$. The photoelectrons thus preferentially absorb photons in excess of the minimum number necessary for ionization at the high intensity where they are created. This explanation of the local yield enhancements near $2h\nu$ and $3h\nu$ should only be viewed as tentative.

In the high-intensity range also the molecular ion H_2^+ or D_2^+ may be ionized by multiphoton absorption. It has been found that the photoionization rate may be enhanced strongly at certain internuclear distances even over the rate of the dissociated species [26]. This effect shows up in the long-wavelength approximation for the MPI process where ionization is treated as a tunnel process in a static electric field. In this model the ionization rate reaches a maximum near an internuclear distance where the active electron just gets localized at one of the ion cores [26]. For H_2^+ or D_2^+ localization of the electron sets in at an internuclear distance $R=6$ a.u. The unperturbed fixed nuclei ionization potential of H_2^+ or D_2^+ at this internuclear separation is 18.5 eV and the photon energy 2.355 eV. This, together with a ponderomotive shift of at least 2.5 eV above 1×10^{14} W/cm^2, may justify treating H_2^+ or D_2^+ MPI already in the long-wavelength approximation with the consequence that preferred ionization is expected near 6 a.u. internuclear separation. H_2^+ or D_2^+ ionization would be a tunnel process which results in a broad unstructured photoelectron spectrum similar to that observed for 1053-nm MPI of H_2 or D_2 (Figs. 5 and 6). Such a tendency of the photoelectron spectrum toward little structure can really be observed at laser pulse peak intensities above 1×10^{14} W/cm^2 (Figs. 3 and 4). A convincing proof for H_2^+ or D_2^+ MPI would be the kinetic energy distribution of the ions. It should resemble the Coulomb repulsion of the bare nuclei near 6 a.u. internuclear distance where ionization is most probable.

These processes [$H(1s)$, H_2^+ MPI] can certainly not be the only reason for the changes observed in the spectra at high intensity since at most 50% (probably less) of the photoelectrons are created by them. Especially the step from 2×10^{14} to 7×10^{14} W/cm^2 is deep in the saturation regime for all processes. Spectral changes may then have as reasons the shift of all processes mainly contributing to the spectrum into the rising edge of the laser pulse and ponderomotive scattering of the free photoelectrons. As shown above, ponderomotive scattering at 7×10^{14} W/cm^2 gives rise to changes in the photoelectron kinetic energy which may reach several eV even for low-energy electrons. The changes in the shape of the photoelectron spectra at high laser intensity cannot yet unambiguously be explained using our experimental results.

C. 1053-nm photoelectron spectra

The photoelectron spectra at 1053-nm excitation wavelength (Figs. 5 and 6) are all recorded at intensities not yet in the saturation regime except possibly the deuterium spectrum at 3.5×10^{14} W/cm^2. At the lowest intensities used, a reproducible structure bound to kinetic energy intervals $[mh\nu,(m+1)h\nu]$ ($m=0,1,\ldots$) with $h\nu=1.177$ eV appears where m enumerates the number of photons absorbed in the ionization continuum. This structure disappears completely above about 8×10^{13} W/cm^2. This is just the intensity where the Keldysh parameter $\gamma=(E^+/2U_p)^{1/2}$ [27] is equal to one. At this intensity a crossover from the multiphoton regime ($\gamma>1$) to the tunnel regime ($\gamma<1$) for photoionization takes place. For $\gamma>1$ a structure on the scale of the photon energy is expected to appear in the photoelectron spectrum while for $\gamma<1$ tunnel ionization should give rise to an almost structureless electron spectrum. This is just what we observe in the photoelectron spectra in Figs. 5 and 6. It was not possible to interpret the structure we see at intensities below 8×10^{13} W/cm^2. One reason for this is the very large ponderomotive potential at this excitation wavelength. This results in the possibility of very many excited states shifting into n-photon resonance with the order n varying over several values. A very congested resonance structure as we observe it is thus to be expected.

Above $\sim 8\times10^{13}$ W/cm^2 laser pulse peak intensity the main contribution to the photoelectron spectra originates in tunnel ionization in the high-intensity part of the pulses. After tunnel ionization the photoelectrons may be assumed to move as free electrons in the laser field, starting with zero velocity after passage of the potential barrier [28], unless they revisit the ion core and scatter. Under these conditions they assume a kinetic drift energy:

$$E_{\mathrm{kin}}=U_p(1+2\sin^2\phi) \tag{7}$$

in a radiation field with time-dependent electric field strength $E(t)=E_0\cos(\omega t+\phi)$ if they start at $t=0$. If no ponderomotive acceleration in the laser beam has to be taken into account (short pulse regime) the photoelectrons are detected with this kinetic energy. In the long pulse regime they gain the full ponderomotive energy and are detected with a kinetic energy $E_{\mathrm{kin}}+U_p$. The most probable emission phase ϕ of the electrons is zero, i.e., at the maximum electric field strength. These electrons then have $E_{\mathrm{kin}}=U_p$ while electrons emitted at $\phi=\pi/4$, i.e., at 70% of the maximum field strength, al-

ready have $2U_p$ drift energy. These energies compare favorably with the energy range where we detect photoelectrons in the measured photoelectron spectra (see Figs. 5 and 6). With relation (1) one calculates as the main contribution to the upper bound for the change in kinetic energy of the photoelectrons by residual ponderomotive acceleration $\Delta E/U_p = 0.027\sqrt{E_0(\mathrm{eV})}$. This shows that especially fast electrons in the photoelectron spectra taken at the highest laser intensity suffer a change in kinetic energy which may reach up to about 5 eV. Ponderomotive acceleration thus has an influence on the shape of the spectra at high intensity and high electron kinetic energy.

A detailed analysis of the 1053-nm spectra is not possible because different processes may contribute besides molecular hydrogen MPI. Tunnel ionization of H_2^+ and $H(1s)$, produced via the possible dissociation channel $H(1s)+H^+$, may contribute. Electrons from these processes will also be broadly distributed in kinetic energy. All that can be said is that there is no isotope effect visible in the photoelectron spectra. The isotope effect in the dissociation fraction at this wavelength (Fig. 2) does not have any influence on the shape of the electron spectra. This may have two reasons: the photoelectron distribution is not sensitive to the differing nuclear dynamics, i.e., purely electronic in origin, or the number of electrons from the process responsible for the isotope effect is small compared to the total number of electrons detected. The first argument may hold if the origin of the isotope effect is H_2^+ or D_2^+ ionization. If, as explained above, H_2^+ or D_2^+ preferentially ionize at a specific internuclear distance, the deuterium nuclei, because of their higher mass, may spend a longer time near that critical distance than the hydrogen nuclei. In this case D_2^+ ionization with subsequent Coulomb explosion is more probable than H_2^+ ionization. This gives rise to the isotope effect in the dissociation fraction. But in this case the contributions from H_2^+ and D_2^+ ionization to the photoelectron spectra would not be different in shape because of equal electronic properties of the ions at the critical internuclear distance.

V. CONCLUSIONS

We extended previous experiments by Zavriyev *et al.* [2] and Yang *et al.* [4,19] on multiphoton excitation of H_2 and D_2 in the IR near 1053 nm and in the visible near 526.5 nm into the short pulse regime. At 526.5 nm this allowed us to identify resonances in the photoelectron spectra which are important for the molecular multiphoton excitation mechanism. In addition the shorter pulse width allowed us to reach higher intensities before saturation of the excitation processes. Resonant H_2 or D_2 ionization dominates MPI at 526.5 nm at intensities between 10^{13} and 10^{14} W/cm^2 with Rydberg states as intermediate resonant states. In the IR we find a crossover from multiphoton to tunnel ionization in this intensity range. The different isotopes give rise to photoelectron spectra with the same shape, meaning that they are determined by the electronic structure of the molecules. An isotope effect is found only in the dissociation fractions at 1053 nm but not at 526.5 nm. Despite getting already detailed information on the H_2 or D_2 excitation mechanisms from the short pulse photoelectron spectra, it is definitely necessary to also measure the kinetic energy distribution of the charged dissociation fragments produced in the interaction process. It will certainly give a better understanding of the molecular dissociation mechanisms which certainly influence the photoelectron spectra. The spectra at 526.5 nm already seem to point at dissociation fragment $[H(1s)/D(1s)]$ MPI. The simple molecular ionization pathway found at 526.5 nm may allow calculations on the light-molecule interaction process to be done even if the processes start in the ground state of the neutral molecule.

ACKNOWLEDGMENTS

We are thankful to Dr. M. Dörr for providing the theoretical intensity dependence of the atomic hydrogen ionization rates and the photoelectron spectrum and Dr. M. P. Kalachnikov for his assistance with the laser system.

[1] J. W. J. Verschuur, L. D. Noordam, and H. B. van Linden van den Heuvell, Phys. Rev. A **40**, 4383 (1989).
[2] A. Zavriyev, P. H. Bucksbaum, H. G. Muller, and D. W. Schumacher, Phys. Rev. A **42**, 5500 (1990).
[3] S. W. Allendorf and A. Szöke, Phys. Rev. A **44**, 518 (1991).
[4] B. Yang, L. F. DiMauro, A. Zavriyev, and P. H. Bucksbaum, Phys. Rev. A **44**, R1458 (1991).
[5] H. Helm, M. J. Dyer, and H. Bissantz, Phys. Rev. Lett. **67**, 1234 (1991).
[6] M. Brewczyk and L. J. Frasinski, J. Phys. B **24**, L307 (1991).
[7] S. L. Chin, Y. Liang, J. E. Decker, F. A. Ilkov, and M. V. Ammosov, J. Phys. B **25**, L249 (1992).
[8] A. Giusti-Suzor, X. He, O. Atabek, and F. H. Mies, Phys. Rev. Lett. **64**, 515 (1990).
[9] A. D. Bandrauk, E. Constant, and J.-M. Gauthier, J. Phys. (France) II **1**, 1033 (1991).
[10] O. Atabek and G. Jolicard, Phys. Rev. A **49**, 1186 (1994).
[11] A. Giusti-Suzor and F. H. Mies, Phys. Rev. Lett. **68**, 3869 (1992).
[12] A. Zavriyev, P. H. Bucksbaum, J. Squire, and F. Saline, Phys. Rev. Lett. **70**, 1077 (1993).
[13] K. Codling and L. J. Frasinski, J. Phys. B **26**, 783 (1993).
[14] A. Giusti-Suzor, F. H. Mies, L. F. DiMauro, E. Charron, and Y. Yang, J. Phys. B **28**, 309 (1995).
[15] D. Normand, L. A. Lompré, and C. Cornaggia, J. Phys. B **25**, L497 (1992).
[16] B. Friedrich and D. Herschbach, Phys. Rev. Lett. **74**, 4623 (1995).
[17] R. R. Freeman, P. H. Bucksbaum, H. Milchberg, S. Darak, D. Schumacher, and M. E. Geusic, Phys. Rev. Lett. **59**, 1092 (1987).
[18] R. S. Gao, P. S. Gibner, J. H. Newman, K. A. Smith, and R. F. Stebbings, Rev. Sci. Instrum. **55**, 1756 (1984).
[19] B. Yang and L. F. DiMauro, Laser Phys. **3**, 398 (1993).
[20] M. Dörr (private communication).
[21] R. Shakeshaft, R. P. Potvliege, M. Dörr, and W. E. Cooke, Phys. Rev. A **42**, 1656 (1990).

[22] H. Rottke, B. Wolff-Rottke, D. Feldmann, K. H. Welge, M. Dörr, R. M. Potvliege, and R. Shakeshaft, Phys. Rev. A **49**, 4837 (1994).
[23] T. E. Sharp, At. Data **2**, 119 (1971).
[24] R. J. Spindler, Jr., J. Quant. Spectrosc. Radiat. Transfer **9**, 627 (1969).
[25] D. E. Ramaker and J. M. Peek, At. Data **5**, 167 (1973).
[26] T. Seideman, M. Yu. Ivanov, and P. B. Corkum, Phys. Rev. Lett. **75**, 2819 (1995); T. Zuo and A. D. Bandrauk, Phys. Rev. A **52**, R2511 (1995).
[27] L. V. Keldysh, Zh. Éksp. Teor. Fiz. **47**, 1945 (1964) [Sov. Phys. JETP **20**, 1307 (1965)].
[28] P. B. Corkum, N. H. Burnett, and F. Brunel, Phys. Rev. Lett. **62**, 1259 (1989).